



Published in final edited form as:

*Proc SPIE Int Soc Opt Eng.* 2020 February ; 11213: . doi:10.1117/12.2549676.

## Development of a new polarized hyperspectral imaging microscope

Ximing Zhou<sup>a</sup>, Ling Ma<sup>a</sup>, Martin Halicek<sup>a</sup>, James Dormer<sup>a</sup>, Baowei Fei<sup>a,b,\*</sup>

<sup>a</sup>The University of Texas at Dallas, Department of Bioengineering, Richardson, TX

<sup>b</sup>University of Texas Southwestern Medical Center, Department of Radiology, Dallas, TX

### Abstract

In this study, we proposed and designed a transmission mode polarized hyperspectral imaging microscope (PHSIM). The hyperspectral imaging (HSI) component is based on the snapscan with a hyperspectral camera. The HSI wavelength range is from 467–700 nm. Polarized light imaging is realized by the integration of two polarizers and two liquid crystal variable retarders (LCVR), which is capable of full Stokes polarimetric imaging. The new imaging device was tested for the detection of squamous cell carcinoma (SCC) in H&E stained oral tissue slides of 8 patients. One normal area and one cancerous area on each slide are selected to make the comparison. The preliminary results indicated that the spectral curves of the Stokes vector parameters (S<sub>0</sub>, S<sub>1</sub>, S<sub>2</sub>, S<sub>3</sub>) of the normal area on the H&E stained oral tissue slides are different from those of SCC in certain wavelength range. Further work is required to apply the new polarized hyperspectral imaging microscope to a large number of patient samples and to test the PHSIM system in different cancer types.

### Keywords

Hyperspectral imaging; polarized light imaging; Stokes vector; head and neck cancer; machine learning

## 1. INTRODUCTION

Polarization imaging is an effective optical imaging technique to explore the structure and morphology of biological tissues through obtaining their polarization characteristics. It can acquire two-dimensional space polarization information of the tissue, which reflects various physical properties of the tissue, including surface texture, surface roughness, and surface morphology information [1, 2, 3, 4, 5]. Hyperspectral imaging, an optical imaging method, which originally was used in remote sensing, recently has been extended to the application in several other promising fields, including biomedical applications [6]. Hyperspectral imaging acquires the spectrum on the pixels of 2D images, then construct the 3D data cube, where rich spatial and spectral information can be obtained. Polarized hyperspectral imaging is a combination of polarization measurement, hyperspectral analysis, and space imaging

\* bfei@utdallas.edu, Website: <https://fei-lab.org>.

technology, which can obtain the polarization, spectral and image information of the object simultaneously [7, 8, 9]. Our group has developed several algorithms for the head and neck cancer detection based on hyperspectral imaging methods, which include principle component analysis (PCA) [10], tensor-based computation and modeling [11], the incorporation of SVM into a minimum spanning forest [12, 13], non-negative matrix factorization (NMF) [14], the combination of super pixels, PCA, and SVM [15], and convolutional neural networks (CNN) [16, 17, 18]. Although polarized light imaging methods have also been adopted in head and neck cancer detection [19, 20, 21, 22, 23], polarized hyperspectral imaging has not been reported for cancer applications.

With the development of information processing technology, a single optical characteristic acquisition method has been unable to satisfy the needs in biomedical imaging for diseases diagnosis. Therefore, the traditional optical imaging methods are constantly improved, so that more information of the tissue can be obtained. This study aims at developing a novel dual-modality microscope, combining polarized light imaging and hyperspectral imaging techniques, for head and neck cancer detection.

## 2. METHODS

### 2.1 System setup

The home-made polarized hyperspectral microscopy operates in the visible spectral bands and was developed for histopathologic analysis (Figure 1). Acquisition of hypercube is realized by a snapscan method. In the snapscan acquisition method, the CCD detectors in the camera move while the sample stays still. Polarimetric imaging is realized by the two polarizers and two liquid crystal variable retarders (LCVR). The system is capable of full Stokes polarimetric imaging, which produces all four components of the Stokes vector. Thus, the system can completely define the transmitted light regarding the intensity and polarization properties.

### 2.2 Data acquisition and processing

Polarized light imaging is realized by the two polarizers and two LCVRs. The system is capable of full Stokes polarimetric imaging, which produces all four components of the Stokes vector. Thus, the system can completely define the reflectance regarding the intensity and polarization properties. The way to calculate the four elements of Stokes vector ( $S_0$ ,  $S_1$ ,  $S_2$ ,  $S_3$ ) is expressed in the following equation:

$$\begin{aligned} S_0 &= I_h + I_v \\ S_1 &= I_h - I_v \\ S_2 &= I_h + I_v - I_{+45} \\ S_3 &= I_{lc} + I_{rc} \end{aligned} \quad (1)$$

where  $I_h$  represent the light intensity measured with a horizontal linear analyzer, in which the retardations of LCVR 1 and LCVR 2 are both set at 0 rad.  $I_v$  represents the light intensity measured with a vertical linear analyzer, in which LCVR 1 is set at 0 rad retardation and LCVR 2 is set at  $\pi$  rad retardation.  $I_{+45}$  represents the light intensity measured with a +45 degrees oriented linear analyzer, in which LCVR 1 and LCVR 2 are

both set at  $\pi/2$  rad retardation.  $I_{lc}$  represents the light intensity measured with left circular analyzer, in which LCVR 1 is set at 0 rad retardation and LCVR 2 is set at  $\pi/2$  rad retardation.  $I_{rc}$  represents the light intensity measured with right circular analyzer, in which LCVR 1 is set at  $\pi$  rad retardation and LCVR 2 is set at  $\pi/2$  rad retardation.

Hyperspectral imaging works simultaneously with polarized light imaging which is realized by snapscan, and the structure of the acquired polarized hyperspectral data cube is shown in Figure 2.

### 2.3 Experimental Design

Before collecting the full-polarization hyperspectral imaging data cube of the tissue slides, validation of the imaging system is a necessary step. We took a quarter wave plate and validated our polarized hyperspectral imaging microscope according to the method proposed in [25]. In the validation experiment, we rotated the quarter wave plate from 0 to 180 degrees at 10 degrees increment, and acquired one polarized hyperspectral data cube under each orientation. As is described in [24], fresh surgical tissue samples were obtained from patients who underwent surgical resection of head and neck cancer. Of each patient, a sample of the tumor, a normal tissue sample, and a sample at the tumor-normal interface were collected. There are totally 192 tissue specimens obtained from 84 patients. Fresh *ex-vivo* tissues are fixed, paraffin embedded, sectioned, stained with haematoxylin and eosin (H&E), and digitized using whole-slide scanning. A boardcertified pathologist with expertise in H&N pathology outlined the cancer margin on the digital slides using Aperio ImageScope (Leica Biosystems Inc, Buffalo Grove, IL, USA).

We chose 8 slides from 8 patients in this preliminary experiment, in which one normal area and one cancerous area are selected on each slide to be imaged under the polarized hyperspectral imaging microscope. The spectral curves of the Stokes vector parameters (S0, S1, S2, S3) are extracted from the images of normal and cancerous areas to make the comparison.

## 3. RESULTS

In order to validate the polarized hyperspectral imaging microscope, we measured the Stokes vector of a quarter wave plate (Thorlabs, AQWP05M-600), and compared our results to the standard result in [25]. As shown in Figure 3, the results demonstrated that the polarized hyperspectral imaging microscope is capable for measuring the Stokes vector of sample under different wavelengths.

We first acquire images of  $I_h$ ,  $I_v$ ,  $I_{+45}$ ,  $I_{rc}$  and then derive Stokes vector parameters S0, S1, S2, S3. Figure 4 demonstrates the synthetic RGB images based on three wavelengths (486 nm, 552 nm, 700 nm) of S0, S1, S2, S3 from a normal area and a cancerous area on the same oral tissue slide. Figure 5 demonstrates the average spectral curves with standard deviations of S0, S1, S2, S3 from 8 different slides of 8 different patients. The spectral curves of S0, S1, S2, S3 are plotted by averaging a random selected ROI of  $100 \times 100$  pixels. The curves for S0, S1, S2, and S3 all have their own peak values, which should be caused by the absorption of hemoglobin and the variance of scattering effect due to the change of nuclei to

cytoplasm ratio. Two sample two tailed T test is applied to the values of  $S_0$ ,  $S_1$ ,  $S_2$ ,  $S_3$  at the wavelength of 486 – 700 nm for the normal and cancer tissue. As shown in Figure 6, there is a significant difference of  $S_0$  ( $P < 0.05$ ) between normal and cancer tissue at the wavelength range of 486 – 700 nm. There is also a significant difference of  $S_1$  and  $S_2$  ( $P < 0.05$ ) at the wavelength range of 550 – 700 nm. Finally, there exists a significant difference of  $S_3$  at the wavelength of 550 – 650 nm.

#### 4. CONCLUSIONS AND DISCUSSIONS

We proposed and developed a polarized hyperspectral imaging microscope system. This is the first polarized hyperspectral microscope based on snapscan with the capability of full Stokes imaging. This is also the first study to use polarized hyperspectral imaging for detection of head and neck cancer.

We tested the imaging system in H&E stained tissue slides of oral cancer patients. The spectral curves (486 – 700 nm) of the Stokes vector parameters ( $S_0$ ,  $S_1$ ,  $S_2$ ,  $S_3$ ) of the normal area on the oral tissue slides are significantly different ( $P < 0.05$ ) from those of the area with squamous cell carcinoma (SCC) at certain wavelength range based on the T test results (486–700 nm for  $S_0$ , 550–700nm for  $S_1$  and  $S_2$ , 550–650 nm for  $S_3$ ). More work need to be performed on the statistical analysis of Stokes vector parameters on more samples and cancer types. It is also worthy to apply machine learning methods in the classification task based on the polarized hyperspectral data cube.

#### ACKNOWLEDGEMENTS

The research was supported in part by the Cancer Prevention and Research Institute of Texas (CPRIT) grant RP190588.

#### REFERENCES

1. Anderson R. Rox. "Polarized light examination and photography of the skin." Archives of dermatology 127.7 (1991): 1000–1005. [PubMed: 2064396]
2. Pierangelo Angelo, et al. "Polarimetric imaging of uterine cervix: a case study." Optics Express 21.12(2013): 14120. [PubMed: 23787602]
3. Rakovi MJ, et al. "Light backscattering polarization patterns from turbid media: theory and experiment." Applied Optics 38.15(1999):3399. [PubMed: 18319938]
4. Liu Bin, et al. "Mueller polarimetric imaging for characterizing the collagen microstructures of breast cancer tissues in different genotypes." Optics Communications 433(2019):60–67.
5. Chang Jintao, et al. "Division of focal plane polarimeter-based  $3 \times 4$  Mueller matrix microscope: a potential tool for quick diagnosis of human carcinoma tissues." Journal of Biomedical Optics 21.5(2016): 056002.
6. Lu Guolan, and Fei B. "Medical hyperspectral imaging: a review." Journal of Biomedical Optics 19.1(2014): 010901.
7. Dong Yang, et al. "Quantitatively differentiating microstructural variations of skeletal muscle tissues by multispectral Mueller matrix imaging" Optics in Health Care and Biomedical Optics VII. Vol. 10024 International Society for Optics and Photonics, 2016.
8. Vasefi Fartash, et al. "Polarization-sensitive hyperspectral imaging in vivo: a multimode dermoscope for skin analysis." Scientific reports 4(2014): 4924. [PubMed: 24815987]
9. Wang Zi, et al. "Polarization-resolved hyperspectral stimulated Raman scattering microscopy for label-free biomolecular imaging of the tooth." Applied Physics Letters 108.3(2016): 033701.

10. Lu Guolan, et al. "Hyperspectral imaging for cancer surgical margin delineation: registration of hyperspectral and histological images" *Medical Imaging 2014: Image-Guided Procedures, Robotic Interventions, and Modeling*. Vol. 9036 International Society for Optics and Photonics, 2014.
11. Lu Guolan, et al. "Spectral-spatial classification using tensor modeling for cancer detection with hyperspectral imaging" *Medical Imaging 2014: Image Processing*. Vol. 9034 International Society for Optics and Photonics, 2014.
12. Pike Robert, et al. "A minimum spanning forest based hyperspectral image classification method for cancerous tissue detection" *Medical Imaging 2014: Image Processing*. Vol. 9034 International Society for Optics and Photonics, 2014.
13. Pike Robert, et al. "A minimum spanning forest-based method for noninvasive cancer detection with hyperspectral imaging." *IEEE Transactions on Biomedical Engineering* 63.3 (2015): 653–663. [PubMed: 26285052]
14. Lu Guolan, et al. "Estimation of tissue optical parameters with hyperspectral imaging and spectral unmixing" *Medical Imaging 2015: Biomedical Applications in Molecular, Structural, and Functional Imaging*. Vol. 9417 International Society for Optics and Photonics, 2015.
15. Chung Hyunkoo, et al. "Superpixel-based spectral classification for the detection of head and neck cancer with hyperspectral imaging" *Medical Imaging 2016: Biomedical Applications in Molecular, Structural, and Functional Imaging*. Vol. 9788 International Society for Optics and Photonics, 2016.
16. Halicek Martin, et al. "Tumor margin classification of head and neck cancer using hyperspectral imaging and convolutional neural networks" *Medical Imaging 2018: Image-Guided Procedures, Robotic Interventions, and Modeling*. Vol. 10576 International Society for Optics and Photonics, 2018.
17. Halicek Martin, et al. "Deep convolutional neural networks for classifying head and neck cancer using hyperspectral imaging." *Journal of biomedical optics* 22.6 (2017): 060503.
18. Halicek Martin, et al. "Optical biopsy of head and neck cancer using hyperspectral imaging and convolutional neural networks." *Journal of biomedical optics* 24.3 (2019): 036007.
19. Lindeboom Jerome A., Mathura KR, and Ince C. "Orthogonal polarization spectral (OPS) imaging and topographical characteristics of oral squamous cell carcinoma." *Oral Oncology* 42.6(2006): 581–585. [PubMed: 16469530]
20. Pahernik S, et al. "Orthogonal polarisation spectral imaging as a new tool for the assessment of antivasular tumour treatment in vivo: a validation study." *British Journal of Cancer* 86.10(2002): 1622–1627. [PubMed: 12085213]
21. Roblyer Darren, et al. "Multispectral optical imaging device for in vivo detection of oral neoplasia." *Journal of Biomedical Optics* 13.2(2008): 024019. [PubMed: 18465982]
22. Manhas Sandeep, et al. "Polarized diffuse reflectance measurements on cancerous and noncancerous tissues." *Journal of Biophotonics* 2.10(2009): 581–587. [PubMed: 19777473]
23. Jung-rae Chung, et al. "Use of polar decomposition for the diagnosis of oral precancer." *Appl Opt* 46.15(2007): 30383045.
24. Lu Guolan, et al. "Detection of head and neck cancer in surgical specimens using quantitative hyperspectral imaging." *Clinical Cancer Research* 23.18 (2017): 5426–5436. [PubMed: 28611203]
25. González Iván Montes, and Bruce Neil C.. "Design and calibration for a Full-Stokes imaging polarimeter" *Unconventional Optical Imaging*. Vol. 10677 International Society for Optics and Photonics, 2018.

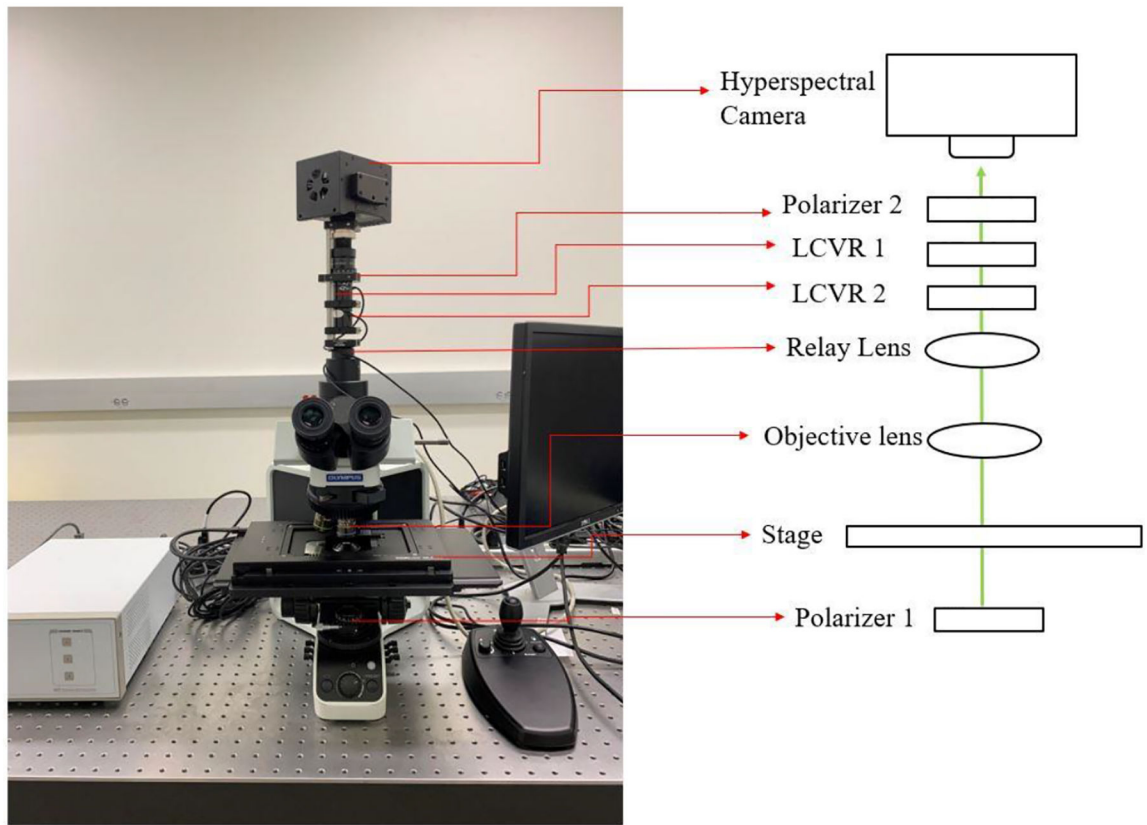


**Fig 1.**  
The setup of the polarized hyperspectral microscope.

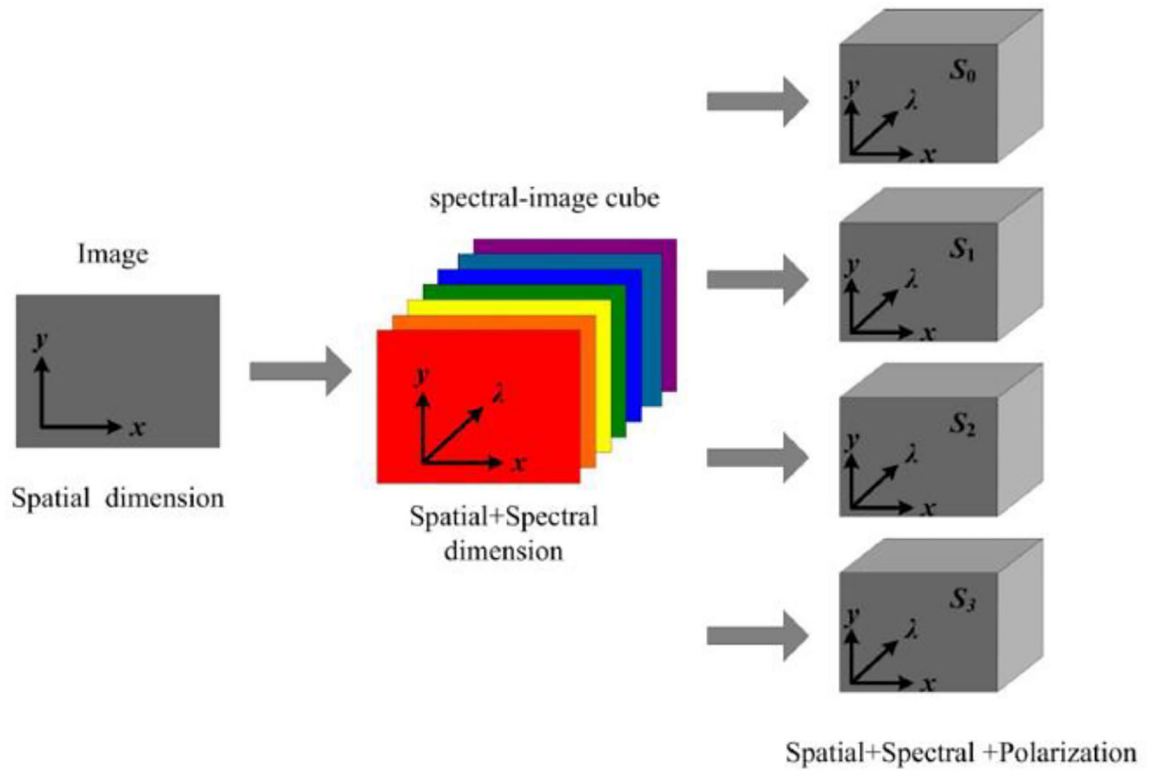


**Fig 2.** Diagram of full-polarization hyperspectral imaging data cube.

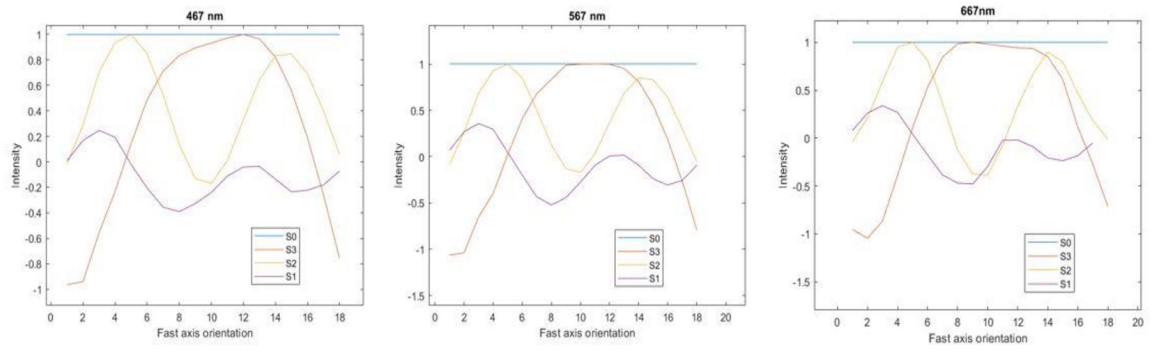


**Fig. 3.**  
The measured Stokes vectors of a quarter wave plate from 0 to 180 degrees orientation at 10 degrees increment at 467 nm, 567 nm, and 667 nm.



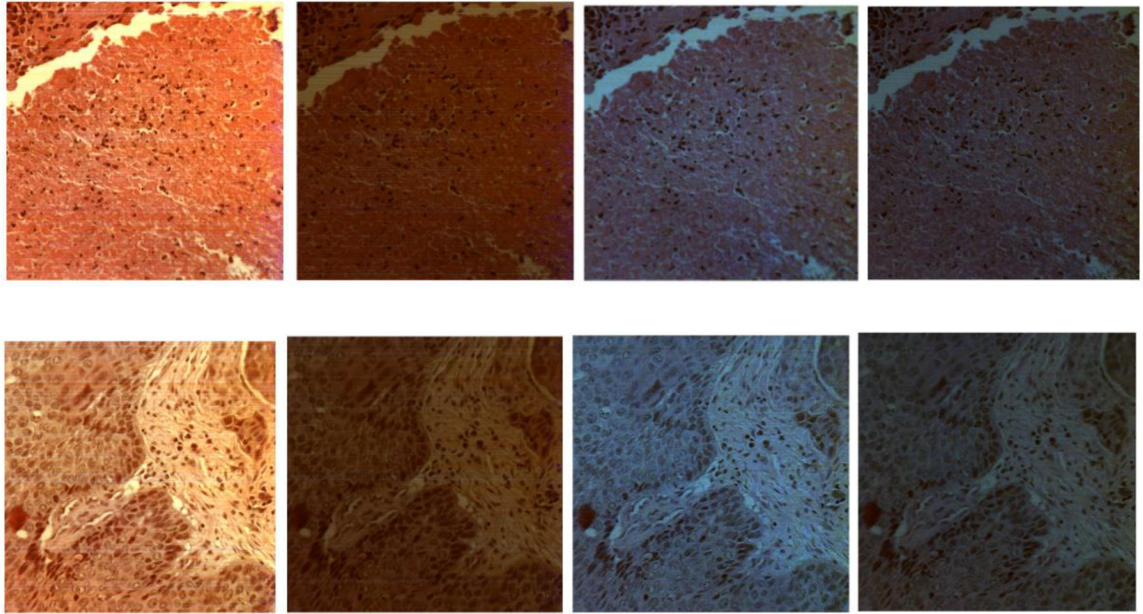


**Fig. 4.** The synthetic RGB images of S0, S1, S2, S3 (left to right) of a normal tissue area (top) and a cancerous tissue area (bottom) on the same oral tissue slide.

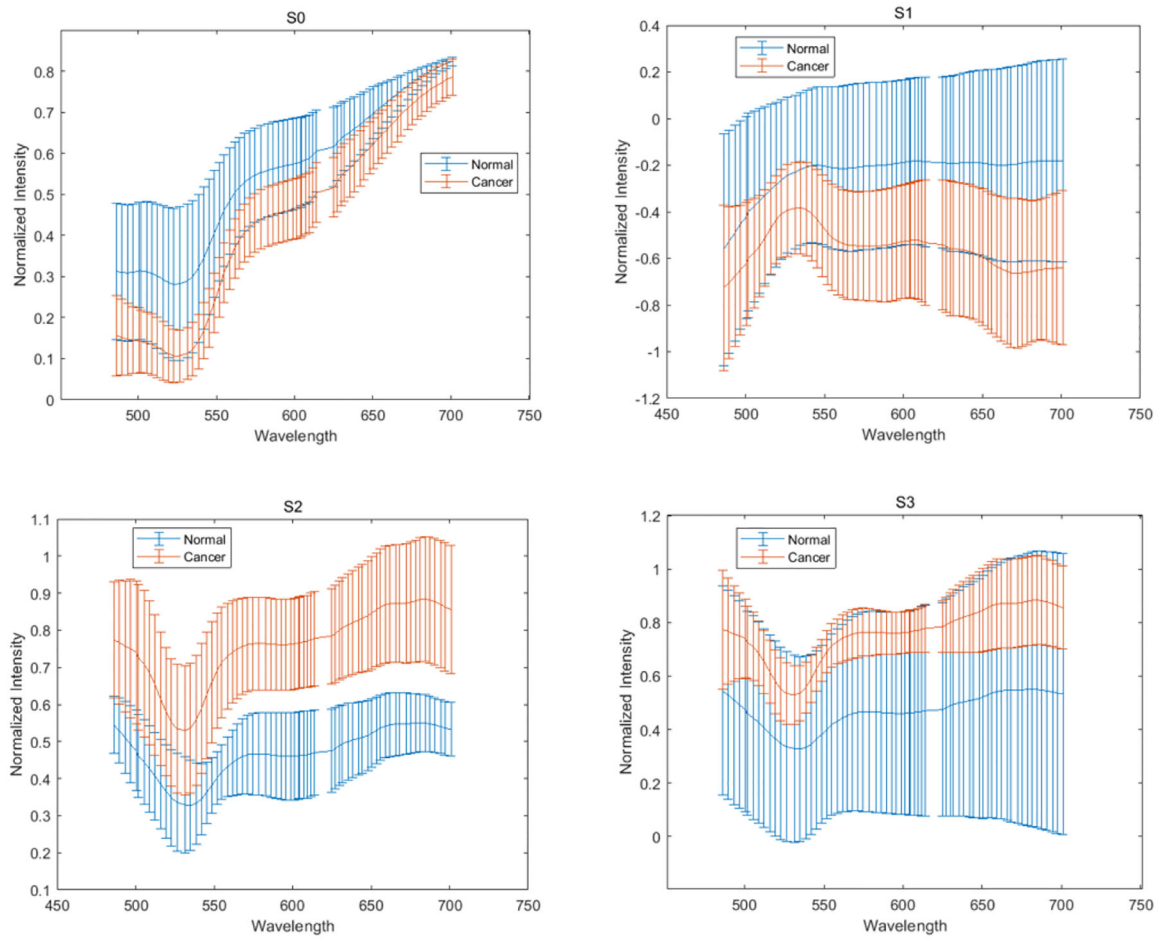


**Fig. 5.** The average spectral curves of S0, S1, S2, S3 with standard deviations from the normal and cancerous areas on eight slides from eight patients.

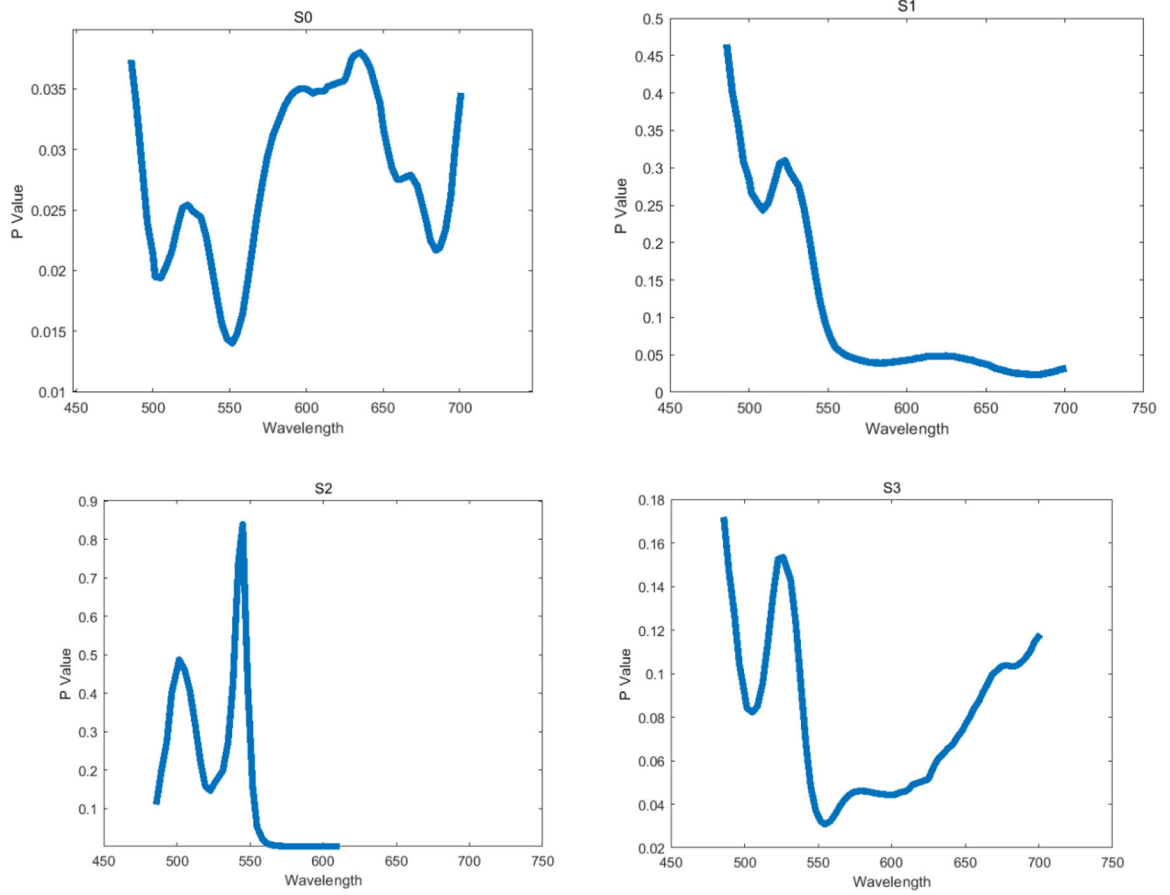


**Fig. 6.** The T test result between normal and cancer tissue for S0, S1, S2, and S3 at 486 – 700 nm.